

Causality for first-order phase transition and its implication on the maximum mass of neutron stars

Asim Kumar Saha* and Ritam Mallick†

*Department of Physics,
Indian Institute of Science Education and Research Bhopal, Bhopal, India.*

Causality is an essential factor in determining the maximum mass of a neutron star. Previous works study causality for smooth equations of state. The density at the core of neutron stars can be a few times nuclear saturation density, where the occurrence of first-order phase transition has not been ruled out. The causality condition for first-order phase transition is characteristically different from that of smooth EOS, which becomes evident in the mass-radius relation. In this letter, we find that equations of state having first-order phase transition, the causality line deviates considerably from the smooth equation of state. Depending on the onset density of phase transition, there is a narrow band in the mass-radius plot, which is available only to the stars having a smooth equation of state. This can have significant consequences in the sense that if some pulsars are to lie in this band, one can rule out the equation of state having first-order phase transition occurring at that particular onset density.

I. INTRODUCTION

Neutron stars (NSs) have proved to be a novel laboratory for testing the theories of high-density matter at low temperatures. The conditions at the cores of NSs are not very easy to achieve in earth-based laboratories, nor can their theoretical calculations be performed from the first principle. In principle, matter at extreme conditions can be studied with quantum chromodynamics (QCD); however, in the intermediate densities (a few times nuclear saturation density $n_0 = 0.16 fm^{-3}$), known nuclear theoretical framework breaks down (like nuclear effective theories and lattice calculations) [1–3]. Till the saturation density chiral effective field (CEF) theories have proven to be effective [4–6]; whereas, at extremely high densities perturbative calculation of QCD (pQCD) works well due to asymptotic freedom [3, 7–9]. However, the only testable laboratories in the intermediate densities are the observations from NSs [10–13]. Studying matter at intermediate densities becomes more interesting as theoretical predictions hint towards the appearance of phase transition (PT) from confined hadronic matter to deconfined quark matter at these densities [2, 14, 15].

The properties of matter are usually described by the equation of state (EOS), which connects different thermodynamic variables of the system [10, 12, 16]. General relativity (GR) connects the EOS with gravity, finally giving a thermodynamic equilibrium condition called the TOV equation [16, 17]. Solving the TOV equation for a given EOS, one obtains the mass-radius of a star. The one-to-one relation of the EOS and M-R sequence curve can be traced by solving the TOV equation for different central densities [16]. There can be minor corrections in the TOV equation due to rotation, magnetic fields and temperature [10, 12, 16, 18–20]; however, the unique

relationship can be traced back from them. Therefore, to obtain the unique EOS that describes matter at high densities several precise mass and radius measurement of pulsars has to be done [10, 12, 21–23].

As determining the exact EOS is still impossible, one looks at different ways of constraining the EOS. For a given EOS, each M-R sequence is characterized by a maximum stable configuration beyond which the star collapses into a black hole. The characteristic maximum mass of the sequence is called M_{TOV} [24, 25]. The M_{TOV} is also a characteristic of the EOS, and works have been done to put bounds on them [25–27]. The EOS can also be expressed in terms of the speed of sound c_s , which is defined as $c_s^2 = \frac{\partial p}{\partial \epsilon}$, where p and ϵ are the pressure and energy density of the corresponding EOS. The speed of sound is bound on the lower end with thermodynamic stability $c_s^2 > 0$ and on the upper end with causality $c_s^2 \leq 1$, where the speed of light is assumed to be 1. However, the non-relativistic models at low density predict $c_s^2 \ll 1$, whereas pQCD predicts that conformality is restored at asymptotic densities where $c_s^2 = 1/3$. The speed of sound at the intermediate densities should interpolate between these two limits. However, the detection of several pulsars in the low [28], intermediate [21, 22] and massive mass range [21–23, 29, 30] hints towards the violation of the conformal limit on c_s^2 is at intermediate densities [31, 32].

Confining NS maximum mass with c_s dates back to the seventies when Rhoades & Ruffini [27] used the causality argument to set an upper limit on the maximum mass. Similar work on the maximum redshift of a neutron star was performed later [33]. Lattimer et al. [26] performed a more detailed and elaborate calculation, where they estimated the upper limit on the maximum mass, its corresponding radius, compactness and redshift. They argued that very accurate mass and radius measurements of even a single star could determine the nature of matter at these intermediate densities.

At high temperatures and low density, the phase tran-

* asim21@iiserb.ac.in

† mallick@iiserb.ac.in

sition (PT) from confined to deconfined matter is most likely a crossover transition [34]. However, there is a possibility that at low temperatures, the PT is of first-order and the existence of a critical point [35]. A first-order PT (FOPT) is associated with a considerable density/energy density discontinuity, although the pressure remains smooth. The causality limit would also differ as FOPT is generically different from smooth EOS. The main objective of this letter is to check the maximum mass-radius (causality) bound for generic EOS having FOPT and how they differ from smooth EOS. If the bounds are substantially different, they can be used to eliminate/predict some of the characteristically different EOS, i.e., smooth from discontinuous existing at the neutron star's core.

The maximally stiff equation of state (EOS), characterized by $\frac{\partial p}{\partial \epsilon} = c_s^2 = 1$, takes the form

$$p = \begin{cases} \epsilon - \epsilon_0 & \text{for } \epsilon > \epsilon_0 \\ 0 & \text{for } \epsilon \leq \epsilon_0 \end{cases} \quad (1)$$

This form allows the Tolman–Oppenheimer–Volkoff (TOV) equation to depend solely on the energy density ϵ , with ϵ_0 as a constant parameter. The single-parameter EOS can be expressed in a scale-free form [26]

$$\begin{aligned} \frac{dw}{dx} &= -\frac{(y + 4\pi x^3(w-1))(2w-1)}{x(x-2y)} \\ \frac{dy}{dx} &= 4\pi x^2 w \end{aligned} \quad (2)$$

where, $w = \frac{\epsilon}{\epsilon_0}$ is the scale-free density, $x = \frac{r\sqrt{G\epsilon_0}}{c^2}$ is the scale-free radius and $y = \frac{m\sqrt{G^3\epsilon_0}}{c^4}$ is the scale-free mass. Extending this treatment to FOPT, we have three parameters: the intercept of the EOS on the energy-density axis ϵ_1 , the onset phase transition density ϵ_{tr} and the width of the discontinuity $\Delta\epsilon$ to express pressure as:

$$p = \begin{cases} 0 & \text{for } \epsilon_1 > \epsilon \\ \epsilon - \epsilon_1 & \text{for } \epsilon_{tr} \geq \epsilon > \epsilon_1 \\ \epsilon_{tr} - \epsilon_1 & \text{for } \epsilon_{tr} + \Delta\epsilon > \epsilon > \epsilon_{tr} \\ \epsilon - \epsilon_2 & \text{for } \epsilon \geq \epsilon_{tr} + \Delta\epsilon \end{cases} \quad (3)$$

where ϵ_2 is given by $(\epsilon_1 + \Delta\epsilon)$. The phase transition, in this case, occurs within the energy density range from ϵ_{tr} to $\epsilon_{tr} + \Delta\epsilon$, with a corresponding transition pressure $p_{tr} = \epsilon_{tr} - \epsilon_1$ as shown in Fig.1. The *crust*, as shown in the schematic diagram, is absent for the scale-free case.

The scale-free variables in this context are $w_i = \frac{\epsilon}{\epsilon_i}$, $x = \frac{r\sqrt{G\epsilon_i}}{c^2}$, $y = \frac{m\sqrt{G^3\epsilon_i}}{c^4}$, where $i = 1, 2$ with G and c representing the gravitational constant and the speed of light in vacuum, respectively. We use geometric units ($G = c = 1$) throughout the paper but report physical radius and mass in units of kilometres and M_\odot , respectively. Numerical integration of equation (2) is performed for various central scale-free densities (w_c). The integration encounters a phase transition for values of w_c lying

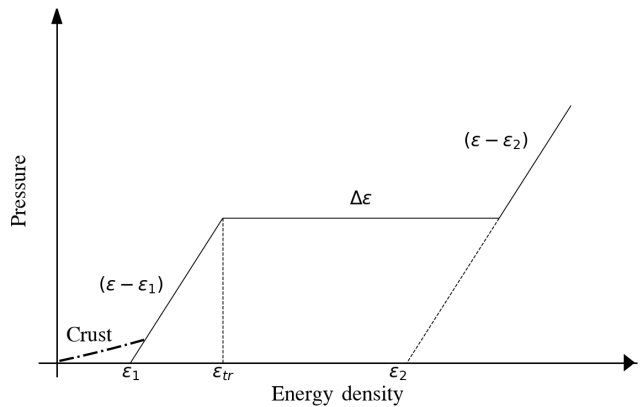


FIG. 1. Schematic diagram of a three-parameter equation of state (EOS), with ϵ_1 , ϵ_{tr} and $\Delta\epsilon$ as the defining parameters, and $\epsilon_2 = \epsilon_1 + \Delta\epsilon$. Here, ϵ_{tr} denotes the onset energy density of FOPT, and $\Delta\epsilon$ represents its strength.

in the second (quark) branch. This transition must be handled by appropriately scaling the variables across the density jump.

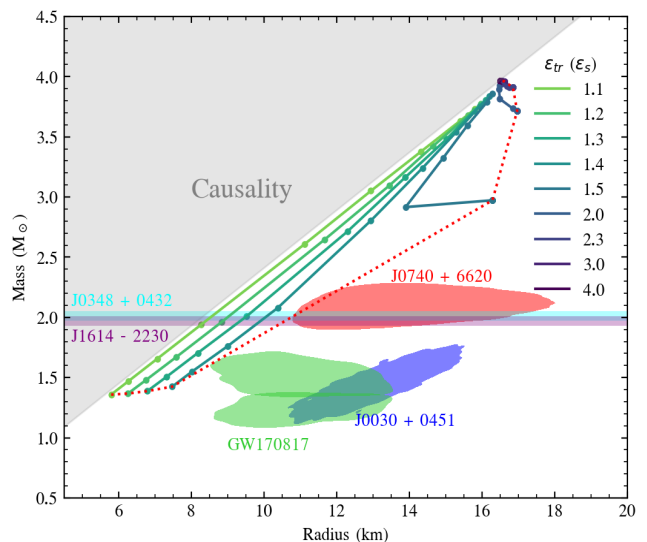


FIG. 2. Causality lines for different values of ϵ_{tr} derived from solving the three-parameter scale-free TOV equations. The figure shows the different causality lines for different onset transition densities, keeping ϵ_1 fixed at 150 MeV. The coloured regions correspond to various astrophysical observations: the red contour represents PSR J0740+6620[36], the blue contour PSR J0030+0451[37], and the green contour GW170817[38]. The cyan band indicates the mass constraint of J0348+0432[39], while the purple band represents J1614-2230[40]. Each scatter point on the causality line marks a stable M_{TOV} for the respective EOS.

The scale-free equation for the three-parameter EOS (Fig.1) having different parameter combinations is solved by varying the three parameters. For a fixed ϵ_1 and with

a given value of ϵ_{tr} , the minimum value of Y the scale-free mass is obtained at the maximum value of $\Delta\epsilon$, while the maximum value of Y occurs at the minimum $\Delta\epsilon$. The maximum value of Y is 0.085. A maximum in Y also corresponds to a maximum in X (scale-free radius) and has a maximum value of ~ 0.25 .

Plotting the bound in the mass-radius diagram gives a clear picture as shown in Fig.2, keeping ϵ_1 fixed at 150 MeV. The grey shaded area shows the causality bound for smooth EOS [26]. In contrast, the causality bound for the FOPT is shown with bold-coloured lines. As the onset density of PT increases, the difference between the two regions (smooth and FOPT) increases in the low mass (and corresponding low radius) region. However, they coincide at higher mass (let's call it M_c) irrespective of the onset density of PT (ϵ_{tr}) and its value being $3.9M_\odot$ (corresponding to a radius of about 16.2 km). Also, after a certain (ϵ_{tr}), we do not get any lower causality bound as we do not get any stable configuration in the second branch, as can be inferred from the abrupt shift of the causality lines starting at $\epsilon_{\text{tr}} = 1.5\epsilon_s$. This is an interesting phenomenon and will be discussed in detail later.

However, ϵ_1 is also a parameter and can be varied. As one increases ϵ_1 , the maximum mass where all the curve coincides M_c decreases, and if ϵ_1 decreases, M_c increases (Fig. 7 in Appendix). As ϵ_1 approaches 0, $M_c \rightarrow \infty$. However, the maximum value of X and Y remains unchanged. As mass and ϵ_1 are related by the scale-free variable Y , they both vary in a way that keeps the maximum value of Y fixed. Similar to the case of X , radius and ϵ_1 vary, keeping the maximum value of X fixed.

For a FOPT, it is generally expected to also produce twin stars. However, solving the scale-free equation (2) alone cannot thoroughly analyze the twins generated. Moreover, recent studies suggest that at low density, the EOS is more or less restricted [41, 42]. Therefore, we turn to the actual numerical solution of Tolman-Oppenheimer-Volkoff (TOV) equations. The maximum masses are of particular interest along these MR sequences, which serve as crucial indicators of the EOS characteristics and allow us to investigate the twin star configurations' stability thoroughly.

To solve the TOV equation, we modify our EOS but still adhere to the causality bound $c_s^2 = \frac{\partial P}{\partial \epsilon} = 1$. Tabulated BPS EOS till $\sim 0.5n_0$ [41] is good enough; whereas till density of $\sim 1.1n_0$, a polytrope of the form $P = Kn^\Gamma$ can be used. The value of K is fixed by matching the lower density BPS EOS, whereas the value of Γ is chosen to represent the stiffest one, spanned by the CET band of Hebeler *et al.* [42] (fig 1).

Incorporating a *crust* into our EOS constrains the parameter ϵ_1 , rendering the other two parameters free. The two parameters defining a FOPT are: ϵ_{tr} and $\Delta\epsilon$. Following the CET band, we impose the causality bound to extend the EOS till ϵ_{tr} . A strong discontinuity then follows till $\epsilon_{\text{tr}} + \Delta\epsilon$. Beyond this, one again has the

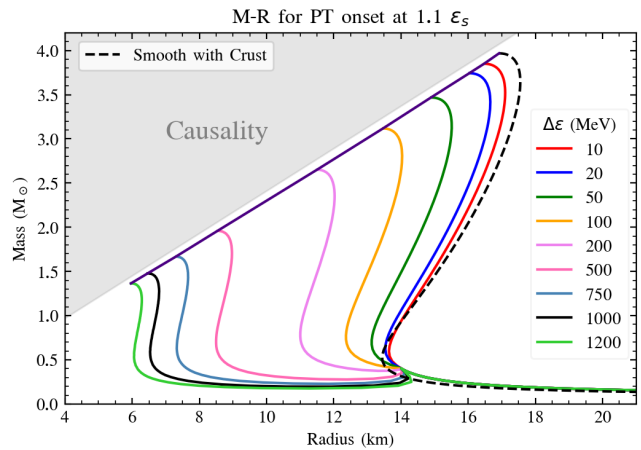


FIG. 3. MR curves for EOS with onset PT density at $1.1\epsilon_s$ and for various $\Delta\epsilon$. The coloured solid lines refer to the MR with FOPT; the dashed line represents the MR curve for maximally compact EOS without any FOPT. The EOS has *crust* at low density.

causality bound to get maximally stiff EOS

$$p = \begin{cases} \text{crust} & \text{for } \epsilon_1 > \epsilon \\ \epsilon - \epsilon_1 & \text{for } \epsilon_{\text{tr}} \geq \epsilon > \epsilon_1 \\ \epsilon_{\text{tr}} - \epsilon_1 & \text{for } \epsilon_{\text{tr}} + \Delta\epsilon > \epsilon > \epsilon_{\text{tr}} \\ \epsilon - \epsilon_2 & \text{for } \epsilon \geq \epsilon_{\text{tr}} + \Delta\epsilon \end{cases} \quad (4)$$

where *crust* refers to the low-density EOS as stated above.

Figure 3 presents the MR sequences for EOS with $\epsilon_{\text{tr}} = 1.1\epsilon_s$ having different values of $\Delta\epsilon$. The grey shaded region marks the causality limit, consistent with the work of Lattimer *et al.* [26]. It is evident that the M_{TOV} for every sequence with FOPT lies below this causality limit. A clear linear correlation is observed between M_{TOV} and $\Delta\epsilon$, with an indigo line connecting the M_{TOV} points, demonstrating an increasing trend in M_{TOV} as $\Delta\epsilon$ decreases. This behaviour is expected, as $\Delta\epsilon$ acts as a softening parameter, directly influencing the stiffness of the EOS. The larger the $\Delta\epsilon$, the softer the EOS becomes, which reduces the star's maximum mass. Consequently, softer EOS results in smaller stars, reinforcing the observed relationship between $\Delta\epsilon$ and the stellar structure.

The trendline of M_{TOV} for $\epsilon_{\text{tr}} = 1.2\epsilon_s/1.5\epsilon_s$ shows a greater deviation from the causality limit (Fig.4), compared to the case of $1.1\epsilon_s$. This pattern of increasing departure continues with larger values of ϵ_{tr} , reflecting the consistent stiffening of the EOS. Additionally, the maximum mass of the first branch also rises as ϵ_{tr} increases. As the onset density increases, we encounter cases where the stability of the second branch breaks down for specific values of $\Delta\epsilon$. This is the case where we encounter unstable twin stars. Twin stars are stars having the same mass but different radii. The twin stars (one in the hadronic branch and one in the quark branch) are separated by a region of unstable stars. The twin stars start to appear

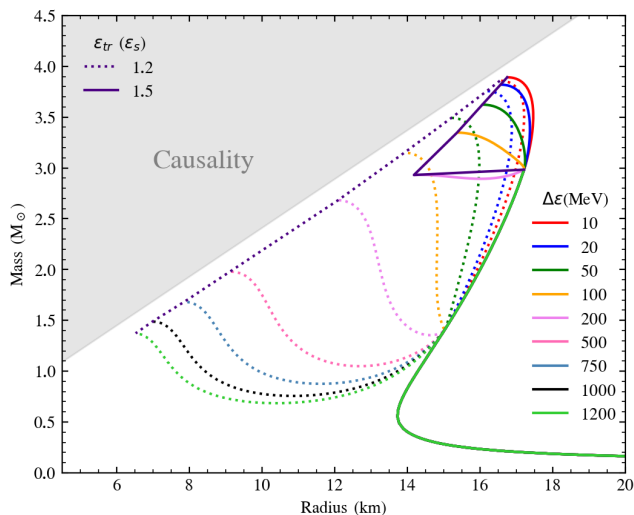


FIG. 4. MR curves for EOS with onset PT density at $1.2\epsilon_s$ (dotted) and $1.5\epsilon_s$ (solid) for various values of $\Delta\epsilon$. The occurrence of stable and unstable twin stars is evident from the figure.

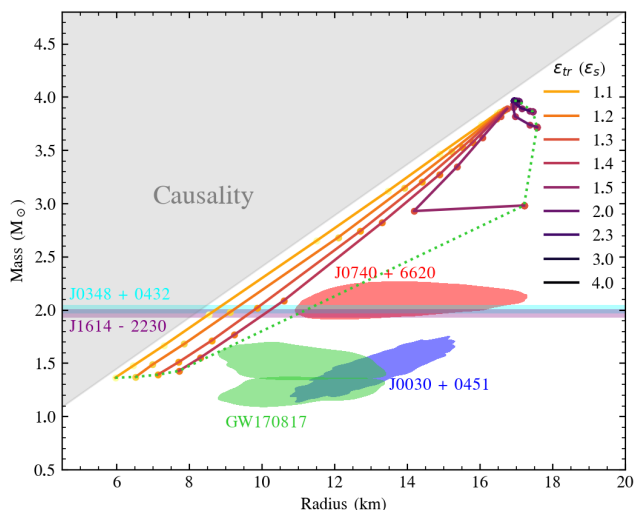


FIG. 5. Causality lines for different values of ϵ_{tr} obtained from solving the TOV equations with a *crust*. The colour codes for observational constraints are consistent with those in Fig. 2. Each scatter point represents a stable M_{TOV} for the respective EOS.

from a lower value of ϵ_{tr} (as can be seen from the $1.2\epsilon_s$ (dotted) case of Fig. 4) but they are stable, and the trendline remains linear. However, for $\epsilon_{tr} = 1.5\epsilon_s$, the lower twin branch does not generate stable twin stars, and we get an abrupt change in the trendline. With further increment in the onset density, we eventually reach a point where ϵ_{tr} causes the stable maximum mass (M_{TOV}) to converge to a degenerate point M_C in the mass-radius space, irrespective of the value of $\Delta\epsilon$.

Figure 5 illustrates the nature of convergence for var-

ious M_{TOV} . Each shade of the inferno line corresponds to a specific value of ϵ_{tr} . The scatter points in the mass-radius space represent stable M_{TOV} values. In the case of $\epsilon_{tr} = 1.5\epsilon_s$, there is a noticeable abrupt shift of the initial scatter point to higher radii. This shift agrees with the scale-free treatment, indicating stable maximum mass for the EOS reached by the first branch while the second branch fails to produce stable stars. Here on, we continue to observe such shifts, signifying that no stable star exists in the second branch for that particular combination of ϵ_{tr} and $\Delta\epsilon$. As we progress to higher values of ϵ_{tr} , the convergence becomes increasingly evident, ultimately reaching a degenerate point M_C (16.902 km, $3.967 M_\odot$).

The convergence of the causality line for different ϵ_{tr} at a high M-R value is similar to what one gets even for scale-free treatment. However, there are two striking differences. FOPT and smooth EOS causality coincide at high mass-radius values for the scale-free treatment. However, the two bound does not coincide with the lower CET bound treatment. This is because the CET does not follow the maximally stiff EOS and, therefore, induces a permanent shift from scale-free treatment. Also, as ϵ_1 is fixed and we only have two parameters, the maximal M_{TOV} is fixed ($3.967 M_\odot$) and does not $\rightarrow \infty$.

In both Fig. 2 and Fig. 5 we have also plotted contours of the present astrophysical bounds. The maximum deviation between smooth and FOPT causality lines happens when $\epsilon_{tr} = 1.4\epsilon_s$. However, neither of the observational contours lies between these two lines. Therefore, those stars are still ambiguous; they can be smooth or have FOPT EOS in them, and there is no way of distinguishing them. The closest observation to the FOPT causality line is the binary star of the GW170817.

In this letter, it is evident that the causality line deviates considerably from that of smooth EOS, whatever the treatment may be, for EOS having FOPT. Depending on the onset density of PT, there is a narrow band in the M-R diagram, which is available only to the stars having smooth EOS. This can have significant consequences because if some pulsars lie in this band, one can rule out EOS having FOPT occurring at that onset density. As the exclusive hadronic band increases with PT onset density, one can quickly rule out FOPT at high density.

ACKNOWLEDGMENTS

The authors would like to thank IISER Bhopal for providing the infrastructure to carry out the research. RM is grateful to the Science and Engineering Research Board (SERB), Govt. of India for monetary support in the form of Core Research Grant (CRG/2022/000663).

DATA AVAILABILITY

This is a theoretical work and does not have any additional data sets.

-
- [1] K. Fukushima and T. Hatsuda, *Reports on Progress in Physics* **74**, 014001 (2010).
- [2] G. Baym, T. Hatsuda, T. Kojo, *et al.*, *Reports on Progress in Physics* **81**, 056902 (2018).
- [3] A. Kurkela, P. Romatschke, and A. Vuorinen, *Phys. Rev. D* **81**, 105021 (2010).
- [4] K. Hebeler and A. Schwenk, *Phys. Rev. C* **82**, 014314 (2010).
- [5] E. Epelbaum, H.-W. Hammer, and U.-G. Meißner, *Reviews of Modern Physics* **81**, 1773–1825 (2009).
- [6] I. Tews, T. Krüger, K. Hebeler, and A. Schwenk, *Phys. Rev. Lett.* **110**, 032504 (2013).
- [7] E. S. Fraga, A. Kurkela, and A. Vuorinen, *The Astrophysical Journal* **781**, L25 (2014).
- [8] T. Gorda, A. Kurkela, P. Romatschke, *et al.*, *Phys. Rev. Lett.* **121**, 202701 (2018).
- [9] B. A. Freedman and L. D. McLerran, *Phys. Rev. D* **16**, 1169 (1977).
- [10] J. M. Lattimer and M. Prakash, *Science* **304**, 536–542 (2004).
- [11] A. L. Watts, N. Andersson, D. Chakrabarty, *et al.*, *Reviews of Modern Physics* **88**, 10.1103/revmodphys.88.021001 (2016).
- [12] F. Özel and P. Freire, *Annual Review of Astronomy and Astrophysics* **54**, 401–440 (2016).
- [13] A. W. Steiner, J. M. Lattimer, and E. F. Brown, *apjl* **765**, L5 (2013), arXiv:1205.6871 [nucl-th].
- [14] E. Annala, T. Gorda, A. Kurkela, *et al.*, *Nature Physics* **16**, 907–910 (2020).
- [15] K. Fukushima and C. Sasaki, *Progress in Particle and Nuclear Physics* **72**, 99 (2013).
- [16] N. K. Glendenning, *Compact stars: Nuclear physics, particle physics, and general relativity* (Springer New York, NY, 1997).
- [17] R. C. Tolman, *Phys. Rev.* **55**, 364 (1939).
- [18] D. Lai and S. L. Shapiro, *apj* **383**, 745 (1991).
- [19] S. Chakrabarty, D. Bandyopadhyay, and S. Pal, *Phys. Rev. Lett.* **78**, 2898 (1997).
- [20] B. Franzon, R. Negreiros, and S. Schramm, *Phys. Rev. D* **96**, 123005 (2017).
- [21] T. E. Riley, A. L. Watts, S. Bogdanov, *et al.*, *The Astrophysical Journal Letters* **887**, L21 (2019).
- [22] M. C. Miller, F. K. Lamb, A. J. Dittmann, *et al.*, *The Astrophysical Journal* **887**, L24 (2019).
- [23] G. Raaijmakers, T. E. Riley, A. L. Watts, *et al.*, *The Astrophysical Journal Letters* **887**, L22 (2019).
- [24] S. Altiparmak, C. Ecker, and L. Rezzolla, *Astrophys. J. Lett.* **939**, L34 (2022), arXiv:2203.14974 [astro-ph.HE].
- [25] V. Kalogera and G. Baym, *The Astrophysical Journal* **470**, L61 (1996).
- [26] J. M. Lattimer, *Annual Review of Nuclear and Particle Science* **62**, 485 (2012).
- [27] C. E. Rhoades and R. Ruffini, *Phys. Rev. Lett.* **32**, 324 (1974).
- [28] V. Doroshenko, V. Suleimanov, G. Pühlhofer, and A. Santangelo, *Nature Astronomy* **6**, 1444 (2022).
- [29] T. E. Riley, A. L. Watts, P. S. Ray, *et al.*, *The Astrophysical Journal Letters* **918**, L27 (2021).
- [30] M. C. Miller, F. K. Lamb, A. J. Dittmann, *et al.*, *The Astrophysical Journal Letters* **918**, L28 (2021).
- [31] I. Tews, J. Carlson, S. Gandolfi, and S. Reddy, *The Astrophysical Journal* **860**, 149 (2018).
- [32] C. Ecker and L. Rezzolla, *Astrophys. J. Lett.* **939**, L35 (2022), arXiv:2207.04417 [gr-qc].
- [33] L. Lindblom, *Astrophys. J.* **278**, 364 (1984).
- [34] D. Alvarez Castillo, S. Benić, D. Blaschke, and R. Lastowiecki, *Acta Physica Polonica B Proceedings Supplement* **7**, 203 (2014).
- [35] M. A. Stephanov, *Prog. Theor. Phys. Suppl.* **153**, 139 (2004), arXiv:hep-ph/0402115.
- [36] T. E. Riley, A. L. Watts, P. S. Ray, *et al.*, 10.5281/zenodo.7096886 (2022).
- [37] M. C. Miller, F. K. Lamb, A. J. Dittmann, *et al.*, 10.5281/zenodo.3473466 (2019).
- [38] B. Abbott, R. Abbott, T. Abbott, *et al.*, *Physical Review Letters* **121**, 10.1103/physrevlett.121.161101 (2018).
- [39] J. Antoniadis, P. C. C. Freire, N. Wex, *et al.*, *Science* **340**, 1233232 (2013), <https://www.science.org/doi/pdf/10.1126/science.1233232>.
- [40] F. Özel, D. Psaltis, S. Ransom, *et al.*, *The Astrophysical Journal* **724**, L199–L202 (2010).
- [41] G. Baym, C. Pethick, and P. Sutherland, *Astrophys. J.* **170**, 299 (1971).
- [42] K. Hebeler, J. M. Lattimer, C. J. Pethick, and A. Schwenk, *The Astrophysical Journal* **773**, 11 (2013).
-

Appendix A: Scale-free TOV for smooth one parameter EOS

The one-parameter maximally stiff EOS, as defined in Equation (1), is shown in Fig.6 (left), where the colour bar represents different values of the parameter ϵ_0 . The corresponding mass-radius (MR) curves for this one-parameter EOS are displayed in Fig.6 (right). Each MR curve has a maximum mass M_{TOV} that aligns along a straight line, referred to as the "causality line." An important observation is that higher values of ϵ_0 result in smaller stars, as increasing ϵ_0 produces a softer EOS. The region above the causality line is shaded in grey, indicating the area excluded

by the causality condition.

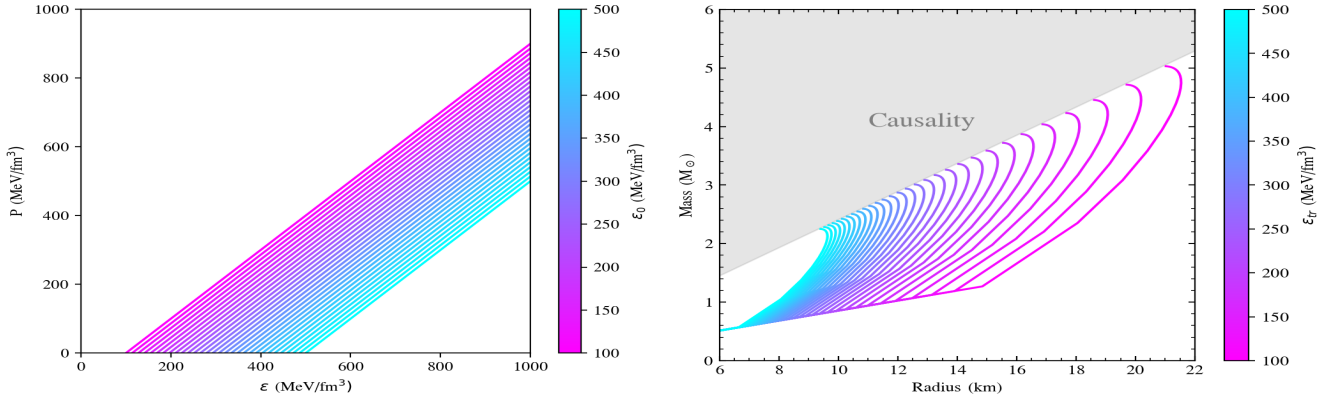


FIG. 6. *Right*: One parameter family of EOS as given by eqn. (1) for various values of ϵ_0 as depicted by the colorbar. *Left*: The corresponding MR curves for the one parameter EOS.

Appendix B: Effect of parameter ϵ_1

The effect of parameter ϵ_1 on the M_{TOV} in the M-R space has been shown in Fig 7. A lower ϵ_1 value leads to higher M_c and larger radius. In contrast, a higher ϵ_1 results in a smaller M_c and smaller radius. The scaling relationship, which indicates that M is inversely proportional to $\sqrt{\epsilon_1}$, is clearly illustrated.

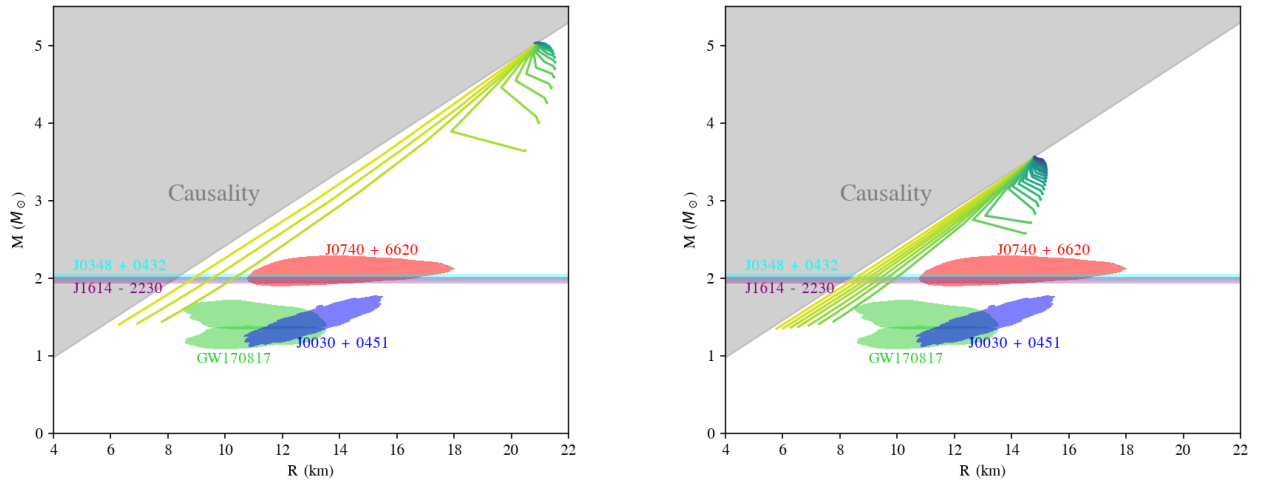


FIG. 7. The panels show mass-radius curves generated using a three-parameter equation of state (EOS) with $\epsilon_1 = 100$ MeV/fm³ (left) and $\epsilon_1 = 200$ MeV/fm³ (right). Observational constraints from pulsars (J0740+6620, J0030+0451, J0348+0432, J1614-2230) and gravitational-wave event GW170817 are also shown, along with the causality limit.